Int. J. Multiphase Flow Vol. 7, pp. 293–309, 1981
Printed in Great Britain

0301-9322/81/030293-17$02.00/0
Pergamon/Elsevier

LIQUID FUEL DROPLETS ENTRAINED IN THE TRANSIENT UNIDIMENSIONAL GAS FLOW IN A PIPE

S. C. Low and P. C. Baruah
Department of Mechanical Engineering, University of Manchester, Institute of Science and Technology, Manchester, England

(*Received* 13 *December* 1979; *in revised form* 26 *September* 1980)

Abstract—Studies of fuel droplets entrained in air flow are deemed to be important in the understanding of fuel transportation and evaporation in the induction system of spark-ignition engines. So far the studies by other authors were restricted to steady air flow, however, the air flow in the induction system is pulsative unsteady air flow. This paper presents a theoretical model and the computational solution for the fuel liquid droplets entrained in the transient unidimensional air flow in a pipe.

INTRODUCTION

The basic functions of the induction system in a gasoline-fuelled spark-ignition internal combustion engine are the metering and mixing of the gasoline and air at a predetermined fuel to air ratio. An ideal induction system will mix all the fuel vapour, liquid fuel and air uniformly and evenly distribute the mixture to the cylinders. The departure from the ideal mixing and distribution adversely affects fuel consumption, exhaust emissions and driveability of the engine. Running the engine at a lean fuel air ratio is regarded generally as the most efficient method of achieving stringent emissions requirement without sacrificing the fuel economy. The leanest mixture conventionally used is limited by the difficulties in achieving uniform air fuel mixing and distributing it evenly to the cylinders. Trayser *et al.* (1969) and Yu (1963) indicated that the complete evaporation of fuel will almost completely eliminate the fuel–air maldistribution among the cylinders. It appears that the studies of evaporation and transportation of the fuel in the induction system are important in relation to cylinder maldistribution and engine driveability under lean burning conditions.

The transportation of single component fuel droplets entrained in a steady air flow in a straight pipe and venturi has been studied by Yun *et al.* (1976) and Lo *et al.* (1977). Boam & Finlay (1979) extended the studies to multicomponent fuels. The air flow in the induction system of a reciprocating internal combustion engine is pulsative. The pulsation is especially noticeable in a single cylinder engine. The aim of this paper is to present a theoretical model and the computer aided solution of the model representing the transportation of fuel droplets entrained in an unsteady gas flow.

ASSUMPTIONS

(1) The unsteady flow is considered one dimensional.
(2) The evaporated fuel is mixed perfectly with the gas and behaves as an ideal gas.
(3) The gas is compressible.
(4) No chemical reaction takes place.
(5) Allowance is made for heat transfer and friction from the pipe wall.
(6) The interaction between droplets and the carrier gas flow is allowed for in the following manner:
  (a) heat transfer between gas and droplets
  (b) drag force between gas and droplets
  (c) evaporation from droplets to the gas.
(7) Slip exists between the droplets and the carrier gas.
(8) The volume occupied by the liquid fuel droplets is small compared with the carrier gas and can be neglected, especially under lean mixture condition.

(9) The fuel droplets are spherical and no temperature gradient is considered within a droplet.

(10) No interaction between droplets, droplets and wall, and no fuel film on the pipe wall is considered.

(11) The fuel considered is of single component.

THEORY

The one dimensional unsteady gas flow equations for the control volume shown in figure 1 are derived as follows:

Continuity equation.

$$\frac{\partial \rho}{\partial t} + \rho \frac{\partial u}{\partial x} + u \frac{\partial \rho}{\partial x} + \frac{\rho u}{F} \frac{\mathrm{d}F}{\mathrm{d}x} - \sum_{i=1}^{n} w_i n_i y_i = 0 \qquad [1]$$

where ρ is the density of carrier gas; u is the velocity of carrier gas; F is the pipe cross-sectional area; t is the time; x is the distance; w_i is the rate of evaporation of droplet i; n_i is the number of droplets i per unit volume of carrier gas; y_i is the fraction of residence time of droplet i in the control volume; and N is the number of droplets in the control volume.

Momentum equation.

$$\frac{\partial u}{\partial t} + u \frac{\partial u}{\partial x} + \frac{1}{\rho} \frac{\partial p}{\partial x} + f \frac{u^2 u 4}{2|u|D} + \frac{1}{\rho} \sum_{i=1}^{N} (w_i u + w_i v_i + F_{di}) n_i y_i = 0 \qquad [2]$$

where p is the pressure of carrier gas; f is the pipe wall friction factor; D is the pipe diameter; v_i is the velocity of droplet i; and F_{di} is the drag on droplet i.

Energy equation.

$$\frac{\partial (C_v T)}{\partial t} + u \frac{\partial (C_v T)}{\partial x} + \frac{p}{\rho F} \frac{\partial (Fu)}{\partial x}$$

$$= f \frac{u^4 2}{D|u|} + q - \frac{1}{\rho} \sum_{i=1}^{N} n_i \left[Q_i - w_i \left(C_{pdg} T_{di} + \frac{v_i^2}{2} - C_v T - \frac{u^2}{2} \right) + F_{di} v_i - u(u w_i - v_i w_i + F_{di}) \right] y_i \qquad [3]$$

where C_v is the specific heat at constant volume for carrier gas; q is the rate of pipe wall heat transfer per unit mass of carrier gas; Q_i is the rate of heat transfer to droplet i; C_{pdg} is the specific heat at constant pressure for fuel vapour; T is the gas temperature; and T_{di} is the temperature of droplet. The empirical equations for the droplet heat transfer, evaporation and drag are identical to the models adopted by Yun *et al.* (1976).

Momentum transfer.

$$F_{di} = C_{di} \frac{\pi}{2} r_i^2 \rho (u - v_i) |u - v_i| \qquad [4]$$

where r_i is the radius of droplet i.

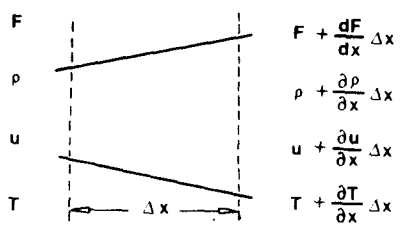

Figure 1.

The drag coefficient C_{di} is based on the Ingebo's (1956) empirical model.

$$C_{di} = 27/\mathrm{Re}_i^{0.84}$$

where

$$\mathrm{Re}_i = \frac{2\rho(u - v_i)r_i}{\mu} \quad \text{for} \quad \mathrm{Re}_i < 400.$$

Heat transfer. The heat transfer model used was initially proposed by Priem & Heidmann (1960)

$$Q_i = h_i(4\pi r_i^2)(T - T_{di})Z_i \qquad [5]$$

where h_i is the heat transfer coefficient which can be evaluated from the Nusselt number proposed by Ranz & Marshall (1952).

Z_i is a correction factor due to the rate of mass transfer from the droplet surface

$$\mathrm{Nu}_i = \frac{2h_i r_i}{k_g} = 2 + 0.6\,\mathrm{Pr}^{1/3}\,\mathrm{Re}_i^{1/2}$$

$$\mathrm{Pr} = \mu\, C_p/k_g$$

where C_p is the specific heat at constant pressure for carrier gas; k_g is the thermal conductivity of carrier gas; and μ is the dynamic viscosity of carrier gas

$$Z_i = \frac{z_i}{e^{z_i} - 1}$$

$$z_i = \frac{w_i C_{pdg}\delta_i}{4\pi r_i(r_i + \delta_i)k_g}$$

$$\delta_i = 2r_i/(\mathrm{Nu}_i - 2).$$

Mass transfer. The mass transfer expression uses the Priem & Heidmann (1960) model.

$$w_i = 4\pi r_i^2 K p_v \alpha \qquad [6]$$

where α is the correction factor which converts the equimolal diffusion to unidirectional diffusion and p_v is the vapour pressure on the droplet surface and calculated by the Reidal–Plank Miller equation from Reid & Sherwood (1966).

$$\alpha = \frac{p}{p_v} \ln\left(p/(p - p_v)\right).$$

K is the mass transfer coefficient and can be calculated from the empirical formula for Sherwood number.

$$\mathrm{Sh} = \frac{2r_i \dfrac{\bar{R}}{M_d}\bar{T}K}{D_g} = 2 + 0.6\,\mathrm{Sc}^{1/3}\,\mathrm{Re}_i^{1/2}$$

$$\mathrm{Sc} = \mu/\rho D_g$$

where $\bar{R}$ is the universal gas constant; M_d is the molecular weight of fuel; D_g is the gas

diffusivity; and $\bar{T}$ is the average film temperature. The equations defining the history of the droplets are calculated as follows:

$$\frac{dv_i}{dt} = F_{di}/(\rho_d 1.33\pi r_i^3) \quad [7]$$

$$\frac{dT_{di}}{dt} = (Q_i - w_i L)/(C_{pdf}\rho_d 1.33\pi r_i^3) \quad [8]$$

$$\frac{dr_i}{dt} = w_i/(4\pi r_i^2 \rho_d) \quad [9]$$

where ρ_d is the liquid fuel density; C_{pdf} is specific heat of liquid fuel; and L is the latent heat of fuel evaporation.

The computational solution

The calculation is mainly based on the method of characteristics. The method of characteristics is a well established numerical method of solving unsteady one dimensional gas flow problems. Jenny (1950) in his pioneering work on one dimensional non-steady flow with friction, heat transfer and area change applied a graphical method to solve the characteristic equations and later a numerical scheme was proposed by Benson *et al.* (1964) to solve a set of unsteady continuity, momentum and energy equations on a computer. The effects of wall heat transfer, wall friction and pipe area change were considered. The present work can be considered as an extension of the work by Benson *et al.* to include fuel droplets into the unsteady gas flow calculation by the method of characteristics.

The momentum, continuity and energy equations of the flow of the mixture of gas and liquid droplets are expressed in the characteristic formulation. Benson *et al.* in their non-homentropic characteristic calculation introduced the Reimann variables (λ and β) as follows:

For the wave characteristic λ along the direction

$$\left(\frac{dx}{dt}\right)_\lambda = u + a$$

$$\lambda = A + \left(\frac{k-1}{2}\right) U$$

$$d\lambda = dA + \frac{(k-1)}{2} dU$$

where a is the speed of sound in the gaseous phase; k is the specific heat ratio of the carrier gas; and A and U are the non-dimensional form of a and u using a reference speed of sound a_{ref}

$$d\lambda = \frac{k-1}{2a_{ref}}\left(-\frac{\Delta_1 dt}{\rho a} - \frac{\Delta_2 dt}{\rho a} - \frac{\Delta_3 dt}{\rho a}\right) + \frac{a}{a_{ref}}\frac{dA_a}{A_a} \quad [10]$$

where Δ_1, Δ_2 and Δ_3 are the parameters defined in [15]–[17], and A_a is the non-dimensional speed of sound at reference pressure, p_{ref}, after isentropic change of A from pressure p.

For the wave characteristic β along the direction

$$\left(\frac{dx}{dt}\right)_\beta = u - a$$

$$\beta = A - \frac{(k-1)}{2} U$$

$$d\beta = dA - \frac{(k-1)}{2} dU.$$

Again the manipulation of [1]–[3] gives

$$d\beta = \frac{k-1}{2a_{ref}}\left(-\frac{\Delta_1\,dt}{\rho a} - \frac{\Delta_2\,dt}{\rho a} + \frac{\Delta_3\,dt}{\rho a}\right) + \frac{a}{a_{ref}}\frac{dA_a}{A_a}. \quad [11]$$

The gas particle path line of the carrier gas travels along the direction $(dx/dt) = u$. For convenience this will be called the gas path line characteristic. The manipulation [1]–[3] gives the change of the property A_a along the gas path line characteristic.

$$dA_a = -A_a\frac{\Delta_1\,dt}{2\rho a^2} \quad [12]$$

$$a = Aa_{ref} = a_{ref}\frac{\lambda+\beta}{2} \quad [13]$$

$$u = Ua_{ref} = a_{ref}\frac{\lambda-\beta}{k-1} \quad [14]$$

$$A_a = a_A/a_{ref}$$

where a_A is the isentropic drop of a to the reference pressure p_{ref} from pressure p as shown in a–s diagram in figure 2.

The notation Δ_1, Δ_2 and Δ_3 used in the preceding equations are now defined

$$\Delta_1 = -X\rho(k-1) \quad [15]$$

$$\Delta_2 = \frac{\rho a^2 u}{F}\frac{dF}{dx} - a^2\sum_{i=1}^{N} w_i n_i y_i \quad [16]$$

$$\Delta_3 = \rho a f\frac{u^2 u4}{2|u|D} + a\sum_{i=1}^{N}(w_i u - w_i v_i + F_{di})\,n_i y_i \quad [17]$$

$$X = q + f\frac{u^4 4}{2|u|D} - \frac{1}{\rho}\sum_{i=1}^{N} n_i y_i\left\{Q_i - F_{di}(u-v_i) + w_i\left[\left(c_{pg}T + \frac{u^2}{2}\right) - \left(C_{pdg}T_{di} + \frac{v_i^2}{2}\right) - (u-v_i)u\right]\right\}.$$

The pressure, temperature and velocity of the carrier gas can be evaluated from λ, β and A_a at any location in the pipe at any instant of time using the following relationships.

$$a = \frac{\lambda+\beta}{2}\,a_{ref} \quad [18]$$

$$u = \frac{\lambda-\beta}{k-1}\,a_{ref} \quad [19]$$

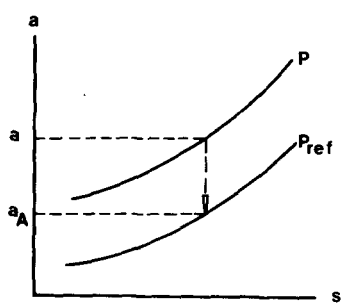

Figure 2.

$$a_A = A_a a_{\text{ref}} \quad [20]$$

$$p = p_{\text{ref}}(a/a_A)^{2k/k-1} \quad [21]$$

$$T = a^2/kR \quad [22]$$

where R is the gas constant of carrier gas.

Equations [10]–[12] form the fundamental equations to be solved by the method of characteristics. These equations relate the wall heat transfer, wall friction, droplets heat transfer, evaporation and drag in a time interval dt to the change of λ, β and A_a along their respective characteristic paths of travel.

The boundary conditions which may vary with time at both ends of the pipe generate a λ characteristic with $\lambda = \lambda(t)$ at one end of the pipe and also a gas path line characteristic from the inflow end of the pipe with $A_a = A_a(t)$ for each predetermined time step. All the λ's, β's and A_a's characteristics travel in their respective characteristic paths within the pipe and the respective $\lambda(t)$'s, $\beta(t)$'s and $A_a(t)$'s values are changed for every time step dt given by $d\lambda$, $d\beta$ and dA_a respectively. Therefore the properties in the pipe at any instant and location can be calculated when the values of $\lambda(t)$, $\beta(t)$ and $A_a(t)$ at the location are known.

The paths of the fuel droplets are represented by a set of droplet path lines. The slope of a droplet path line on $x-t$ diagram is given by

$$\frac{dx}{dt} = v_i.$$

As there is a large number of fuel liquid droplets in the pipe, it would be quite impractical to represent each droplet by a single path line. For convenience, we assume that only one initial droplet size is injected into the pipe. Of course the droplet size will change due to evaporation within the pipe. A single droplet path line is used to represent a group of fuel droplets very close to each other and occupying a particular section of the pipe at a particular instant. In order to define all the droplets in the pipe, M number of droplet path lines are introduced. These droplets paths lines are shown schematically in figures 3 and 4.

The dots in the pipe shown in figure 3 represent the droplet path lines at a particular instant. All the fuel droplets in each shaded section are represented by one droplet path line. There are eleven droplet path lines shown in the figrue. The droplets in each shaded section are assumed to have the same radius, temperature and velocity. The assumptions are true when the droplets are not very far away from each other.

Figure 4 shows the locus of the droplet path lines in the time distance diagram for one

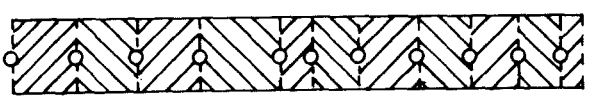

Figure 3. The droplet path lines in a pipe.

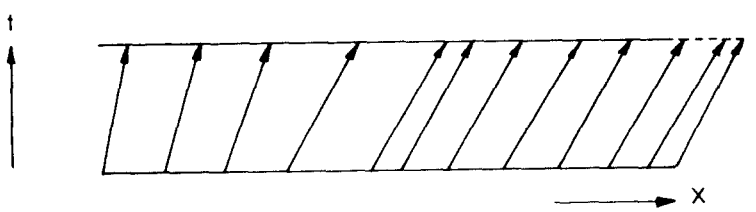

Figure 4. The loci of droplet path lines in one time step.

particular time step. Under the assumptions of operating fuel–air mixture in an engine and small time step, the gas velocity, temperature and pressure of the droplets are subjected to very small changes within the time step due to the droplet heat transfer, evaporation and drag. These changes are of little significance in the calculation of the droplets history within the time step. Therefore the temperature, pressure and velocity of the carrier gas at the beginning of the time step are used for the calculation of droplet pathlines within the time step.

Figure 5 superimposes the loci of the gas path lines onto the droplet path lines in the time distance diagram. When the gas path lines is in contact with the droplet path lines, the fuel vapour picked up by the gas is recorded on the gas path line in the form of mole ratio of fuel and air. The gas temperature, pressure and velocity at each droplet path lines are calculated by interpolation between the gas path lines at the beginning of the time step R. The derivatives of T_{di}, v_i and r_i are calculated by [7], [8] and [9] and eventually the droplet T_{di}, v_i and r_i at the end of the time step are then calculated. The Bulirsch & Stoer (1966) extrapolated integration scheme is used in the droplet history calculation.

Each droplet path line registers the following properties:

(1) Droplet temperature T_{di}.
(2) Droplet velocity v_i.
(3) Droplet radius r_i.
(4) Droplet location x_{di}.
(5) Number of droplets represented by the path line.
(6) The rate of the droplet evaporation w_i.
(7) The droplet drag coefficient C_{di}.
(8) The rate of the droplet heat transfer Q_i.

The above properties can be calculated by [4]–[9] at the end of the time step for all droplet path lines. After the properties of the droplet path lines have been evaluated, then the interaction between the characteristics λ, β, A_A and the droplets is considered. Figure 6 shows the loci and the interaction of the droplet path lines and the characteristics within one time step. The modification of $\lambda(t)$, $\beta(t)$ and $A_a(t)$ values due to the interaction can be evaluated directly from [10] to [12].

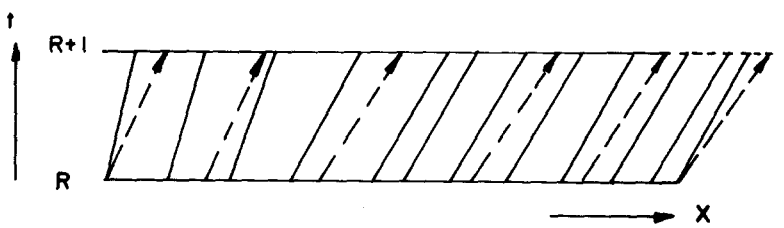

Figure 5. The loci of gas path lines superimposed on the locus droplet path lines for one time step.

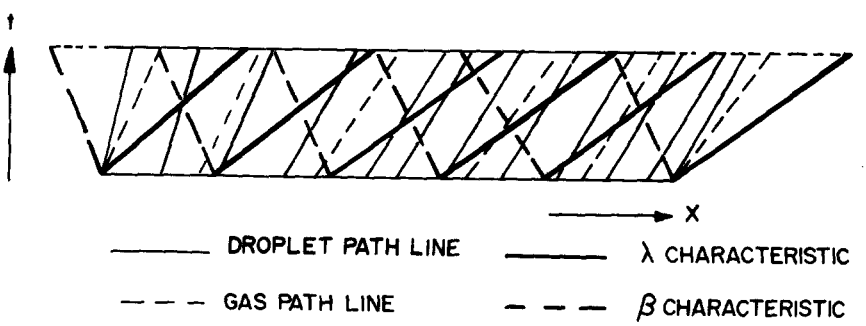

Figure 6. The interaction between λ, β and A_a characteristics.

The algorithm or the proposed numerical scheme for each time step of calculation is given below:

(1) Calculate the histories of all the droplet path lines by [4]–[9] within the time step.

(2) Calculate the entropy measure of all the gas paths lines by [12].

(3) Calculate the λ and β characteristics by [10] and [11] respectively.

(4) Calculate the λ, β and A_a characteristics at the pipe ends by quasi-steady boundary conditions as proposed by Benson *et al.* (1964).

(5) Introduce a droplet path line into the pipe end where fuel is injected.

The calculation proceeds from one time step to the other and the Riemann variables λ and β are calculated and stored at equidistant mesh points along the pipe. However, A_a's of the gas path lines, are calculated along their path characteristics and stored with reference to the distance from one end of the pipe. Both the storages of the λ, β and A_a characteristics described above are exactly same as the method proposed by Benson *et al.* (1964). The droplet path lines are stored similar to the gas path lines.

RESULTS AND DISCUSSION

The unsteady droplet and air flow model was applied to the air fuel mixture flow through a pipe of 0.2 m length and 0.04 m dia. and in this section the results are presented and analysed. One end of the pipe is connected to a constant pressure reservoir with a pressure of 1.0 bar and temperature 300 K. The other end of the pipe is covered by a diaphragm. When the diaphragm is fractured the pipe end will be exposed to a pressure of 0.986 bar. The air in the pipe is initially at rest and the properties are identical to the reservoir. Iso-octane fuel at 280 K and zero longitudinal velocity is injected at the reservoir end of the pipe. The mass flow rate of the injected fuel is

$$\dot{m} = 0.004\, t/0.01 \text{ kg/s} \quad \text{for} \quad t \leq 0.01 \text{ s}$$

$$\dot{m} = 0.004 \text{ kg/s} \quad \text{for} \quad t > 0.01 \text{ s}.$$

Immediately after the fracture of the diaphragm both air and fuel begin to flow. The transient gas pressure and velocity are shown in figures 7 and 8 respectively. An expansion wave is created at the pipe end fitted with the diaphragm and travels upstream causing the sharp pressure drop near the beginning of the discharge period. As soon as the expansion wave arrives at any location the air particle velocity there is increased as shown in figure 8. Soon after the expansion wave reaches the pipe end upstream, a compression wave is sent downstream causing a sharp rise in pressure along its path of travel. The travel of pressure waves in the pipe leads to the consecutive stepped rise of air particle velocity. After a while, the waves from both ends of the pipe tend to cross each other. As a result a double wave is formed which smooths out the pressure time relationship in the later period of the transient air discharge.

The trend of these transient pressure and velocities predicted by the proposed unsteady droplet and air flow model are confirmed by the unsteady results predicted by the characteristics method by Benson *et al.* (1964) without fuel injection. The comparison is given in figures 9 and 10. No significant difference in the timing of the wave travel is observed between the two cases. However, it is noticed that the transient pressures are slightly damped by the fuel droplets when the waves travel from one end of the pipe to the other. The comparisons in figure 10 indicate that the rise of transient air velocity is slower when fuel droplets are present. The resulting steady state air velocity within the pipe is also slower in the case with fuel injection.

It has been found that the above effects on the transient behaviour of the gas flow caused by the presence of fuel droplets are more severe with either smaller droplet size or higher fuel to air ratio.

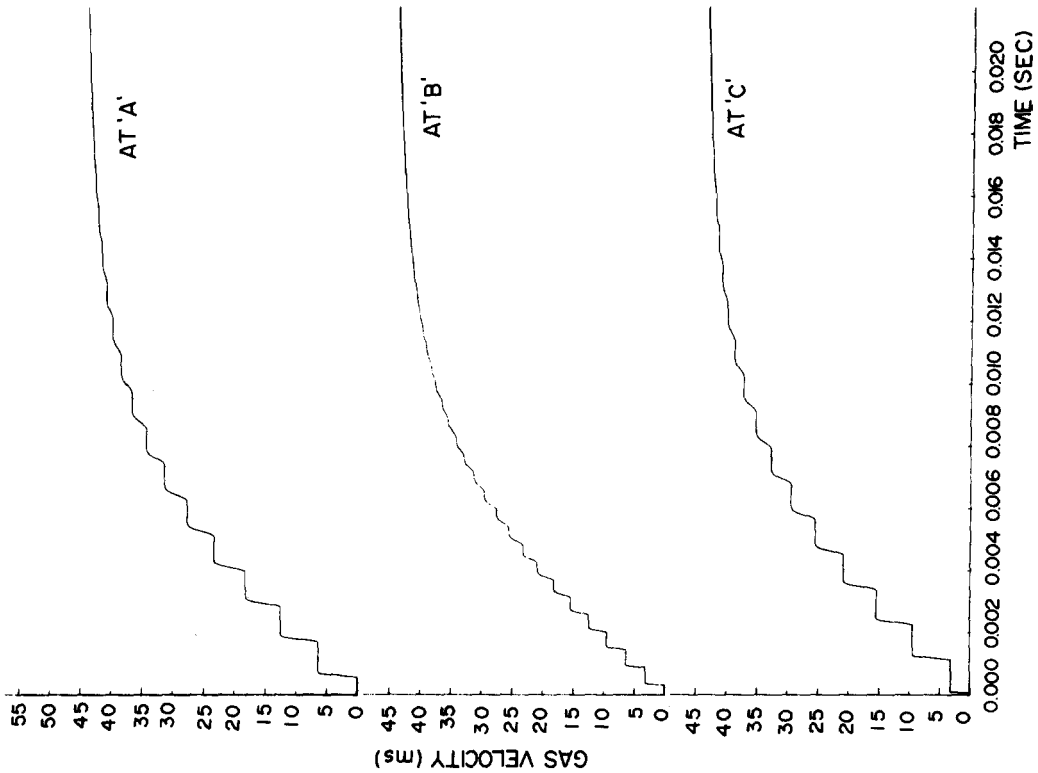

Figure 8. The transient gas velocity at different pipe location.

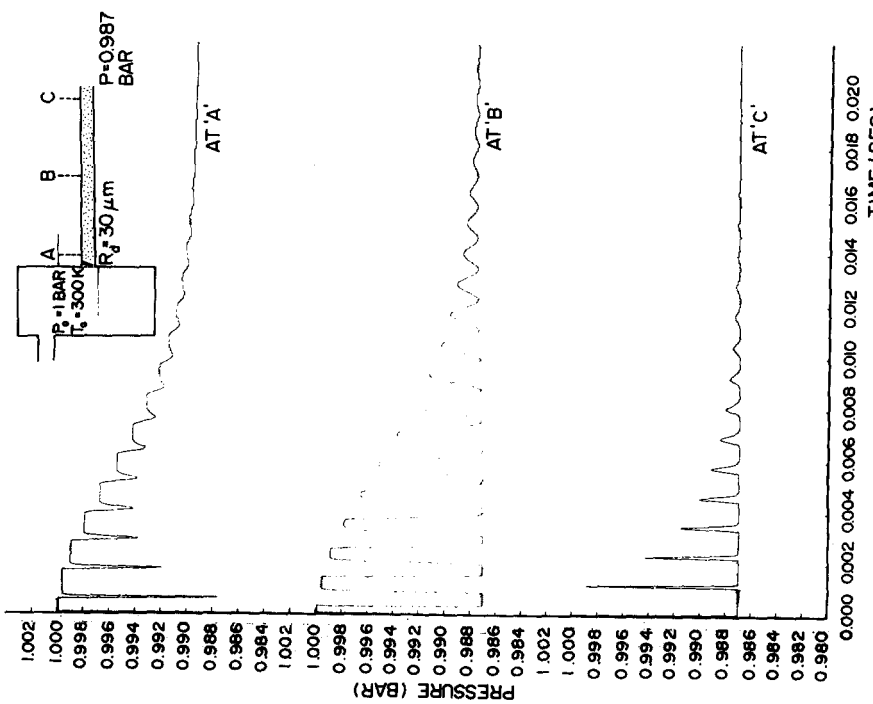

Figure 7. The transient pipe pressure at different location.

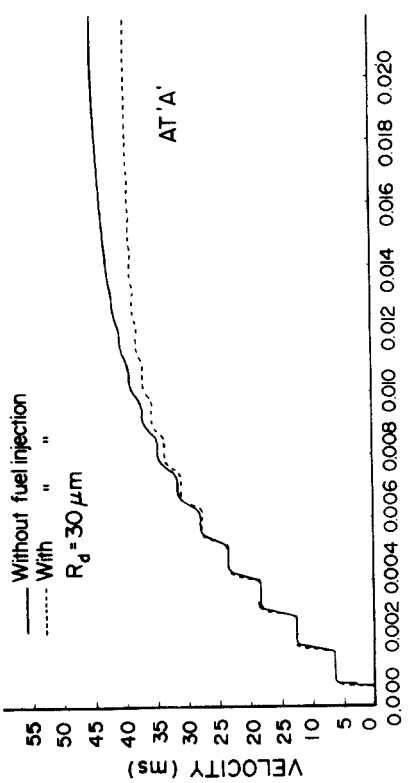

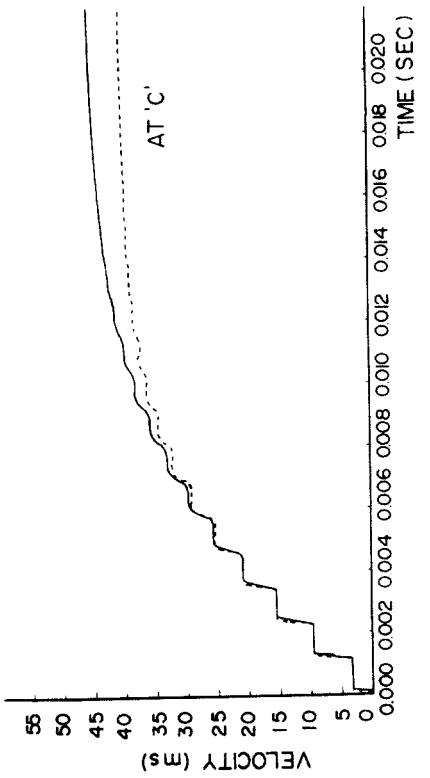

Figure 10. The comparisons of transient gas velocity.

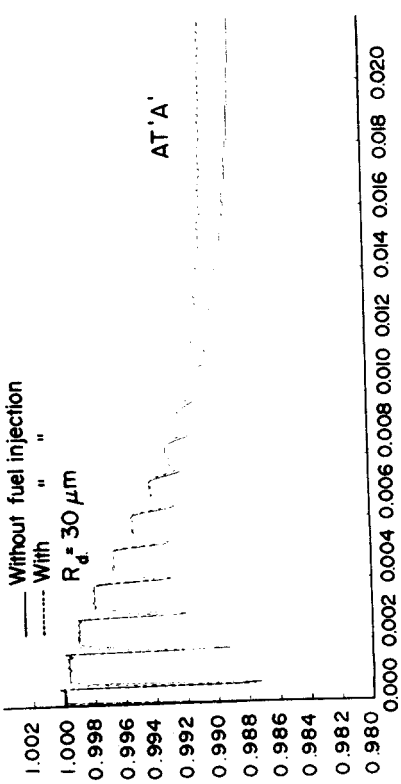

Figure 9. The comparisons of transient gas pressure.

The transient fuel vapour to air ratios at the pipe exit with different initial droplet radius are presented in figure 11. Generally, the shape of the curves can be subdivided into three sections given below:

(1) Steep rise period.
(2) Gradual rise period.
(3) Gradual fall period.

Initially the pipe is not filled with any fuel droplets. After the fuel begins to flow, the fuel droplets progressively fill the pipe. In this particular test the air velocity increases and is always faster than the droplet velocity at any particular pipe location. During this period the fuel vapour being picked up by the successive gas path lines rapidly increases causing the steep rise period of the fuel vapour to air ratio at the pipe exit. After the fuel droplets have almost filled the pipe the rate of fuel injection is still allowed to increase wth respect to time causing the period of gradual rise in the discharged fuel vapour to air ratio. The rate of fuel injection remains constant after 10 ms, but the air velocity after this moment still continues to increase. As a result, the time available for the air in contact with the droplets decreases and hence the gradual drop of the exit fuel vapour to air ratio is observed.

The droplet path lines each representing a group of droplets in a finite pipe section used in the proposed model artificially create discontinuity of fuel droplet properties within the pipe because of the nature of stepped representation. This effect is revealed in the slight discontinuity of fuel vapour to air ratio calculated at the pipe exit, as given in figure 11. This effect can be more severe as shown in figure 12 with lesser number of droplet path lines.

The trace of the properties of a droplet path line along the pipe is presented in figure 13. The

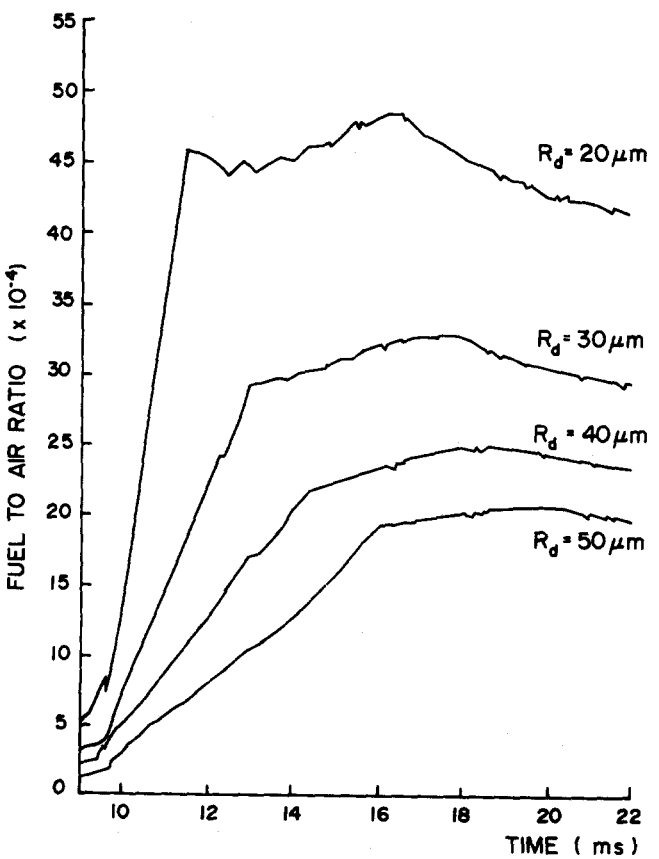

Figure 11. Evaporated fuel to air ratio at the pipe exit.

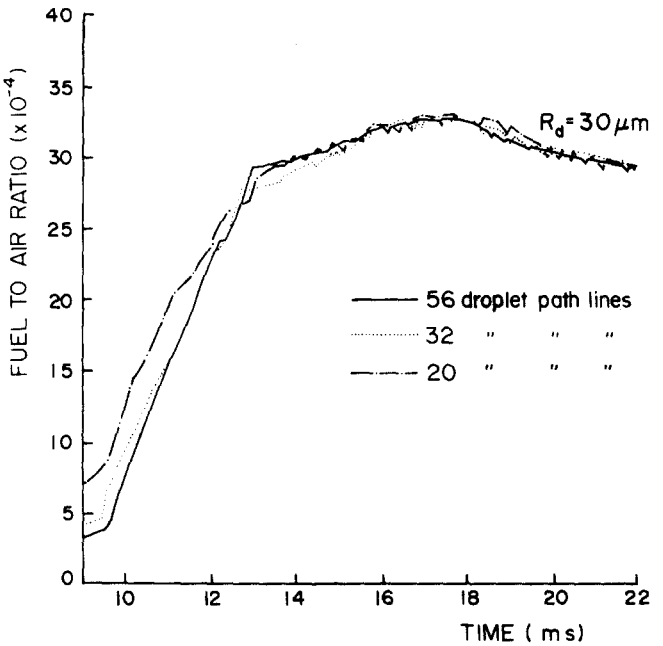

Figure 12. Comparison of the evaporated fuel to air ratio predicted at the pipe exit using different droplet path line number.

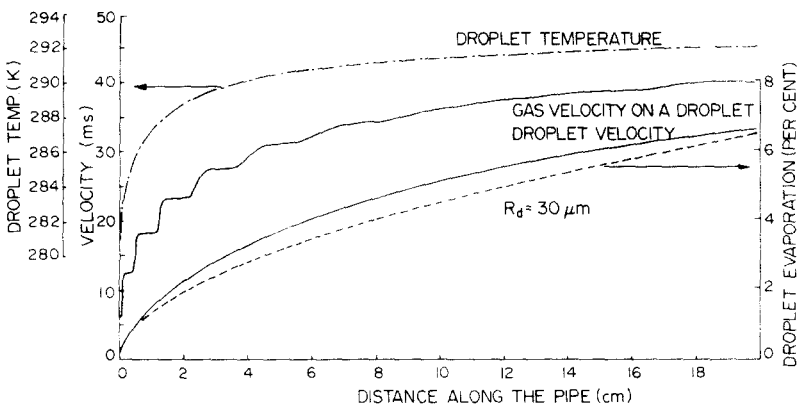

Figure 13. Properties of a droplet path line along the pipe.

droplet temperature rises rapidly in the first 4 cm of the pipe. The stepped air velocity change only causes slight wavering affect on the droplet velocity owing to the droplet inertia. As the air velocity increases progressively a velocity difference is maintained between the air and the droplet throughout the pipe which is favourable to fuel evaporation.

The gas temperature along a gas pathline, shown in figure 14, is wavy throughout the pipe. There is a relatively fast drop in the gas temperature initially, where the air experiences a relatively greater amount of fuel evaporation at the pipe entrance. This is confirmed by the fuel vapour to air ratio curve given in the same diagram. A downwards trend of the gas temperature is observed in the diagram. This is due to the combined effects of fuel evaporation and gradual gas velocity increase along the pipe.

The effects of the number of gas and droplet path lines and meshes on the computer run time and accuracy of the prediction are now studied. It is found that the number of droplet path

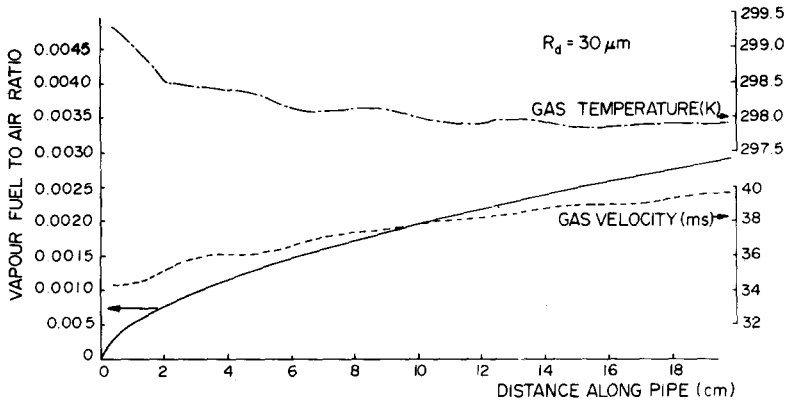

Figure 14. Properties of a gas path line along the pipe.

lines significantly affects the computer run time. More droplet path lines are required when greater extent of the fuel air stratification occurred along the pipe. This can be seen in figure 12 where greater error occurred at the steep portion of the curve when lesser number of droplet path lines is used. The number of meshes used per pipe does not affect the accuracy of the calculation but a higher number increases the run time by a great deal. Lesser number of gas path lines tends to smooth out the details of the properties of the carrier gas. Its effects on the predicted fuel vapour to air ratio can be seen from figure 15.

In the present test the unsteady behaviour of air and fuel flow will finally settle down to steady state. At this instance, the comparison of the fuel vapour to air ratio calculated separately from the gas path lines (from gas calculation) and the droplet path lines (from drop calculation) along the pipe is presented in figure 16. This comparison shows that the fuel vapour to air ratios calculated from both means agree extremely well.

The steady state results calculated by the characteristics model are compared with the

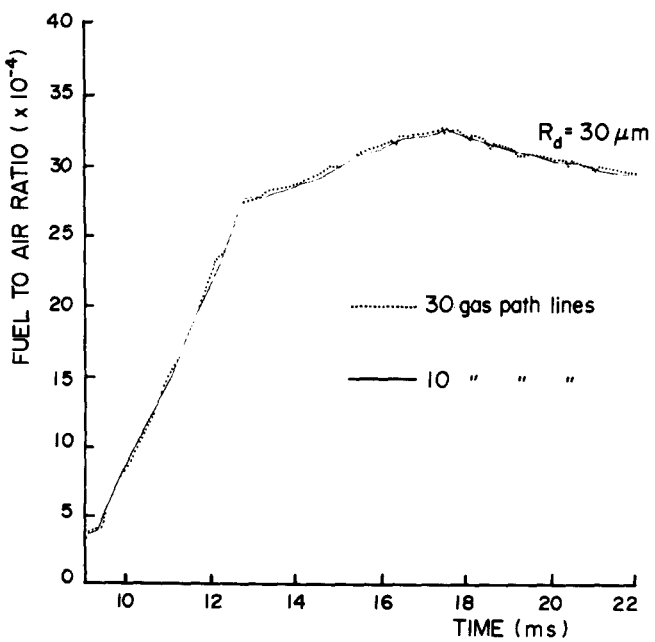

Figure 15. Comparison of the evaporated fuel to air ratio predicted at the pipe exit using different gas path line number.

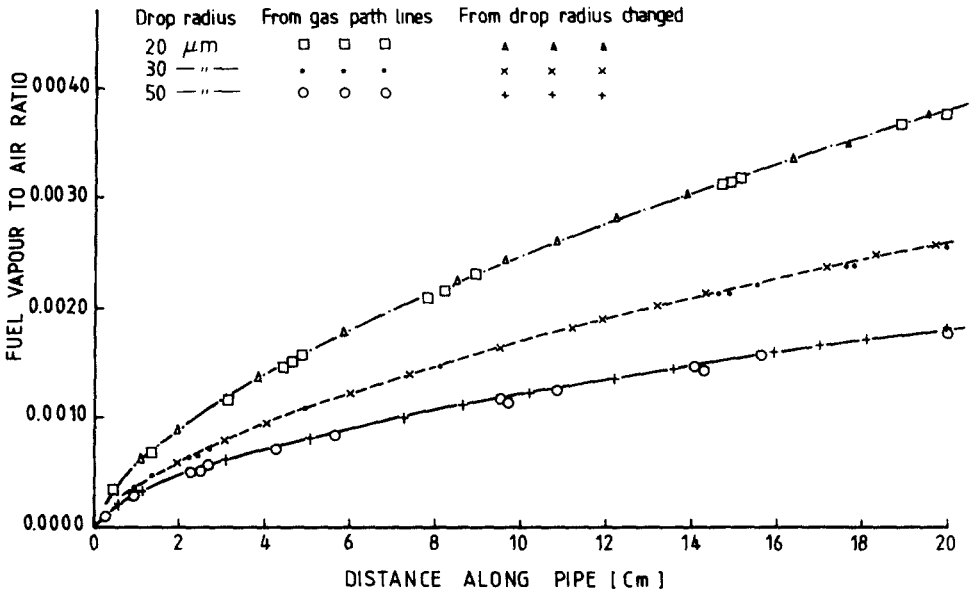

Figure 16. Fuel vapour to air ratio calculated from both gas and droplet path lines using the characteristics model.

results generated by the steady state model by Yun *et al.* (1976) in figures 17–20. Generally speaking the comparisons, shown in figures 17–20 show excellent agreement.

These comparisons confirm that the proposed characteristics model, which introduces three sets of characteristics interacting with a set of fuel droplet path lines, is a correct approach, at least under steady state condition to solve this kind of two-phase flow problem. However, the newly proposed characteristics model is much more superior as compared with the steady model. The former is capable of handling a two-phase flow of unsteady fuel droplets and air flow where the latter is completely incapable of handling unsteady phenomenon.

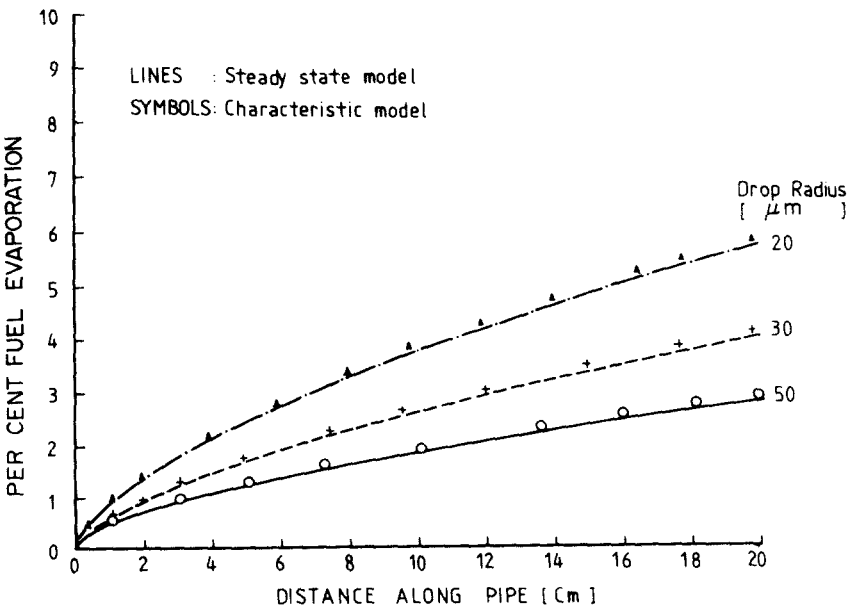

Figure 17. Comparison of fuel evaporation between the steady state and characteristics model.

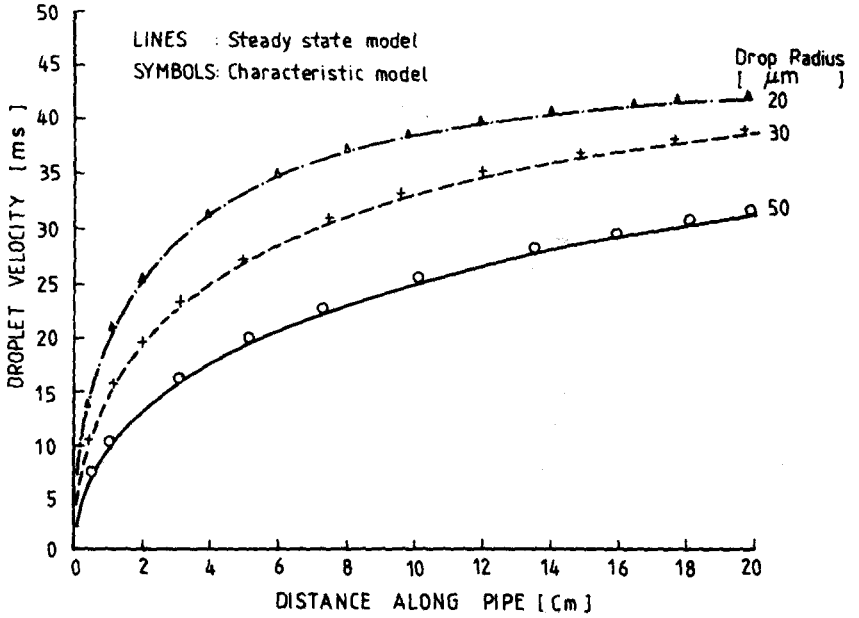

Figure 18. Comparison of predicted droplet velocity between steady and characteristics model.

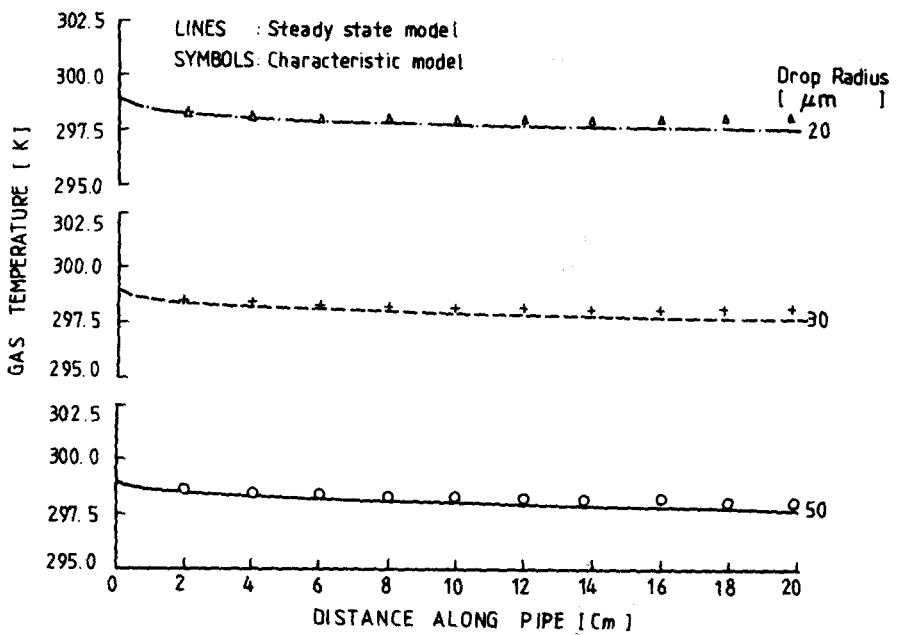

Figure 19. Comparison of gas temperature between the steady state and characteristics model.

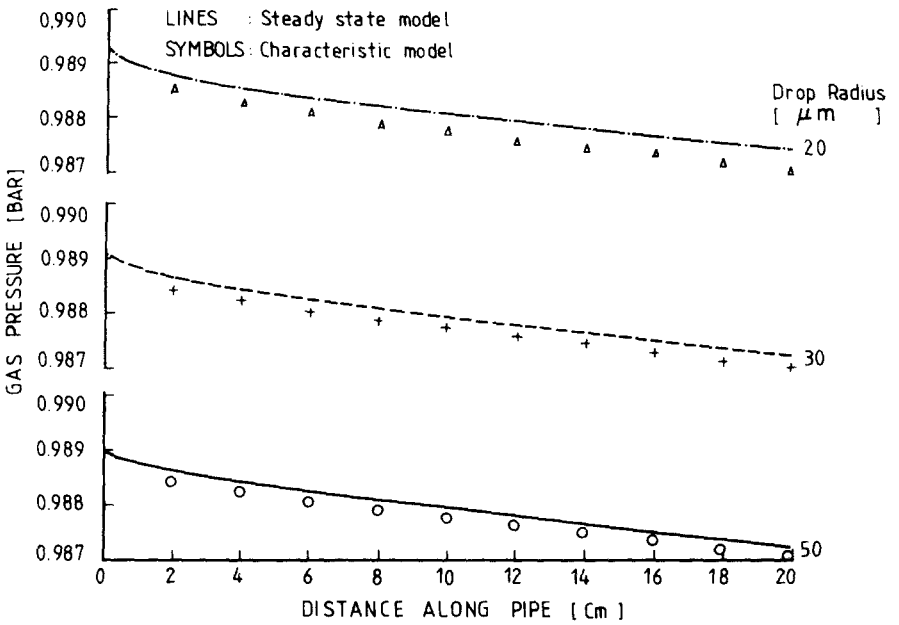

Figure 20. Comparison of gas pressure between the steady state and characteristics model.

CONCLUSION

A numerical scheme for the calculation of an unsteady flow of air (gas) and fuel (liquid) droplet in a duct is presented. The technique uses the method of characteristics which handles a set of equations physically representing the waves travelling upstream and downstream of the duct, and the travel of gas particles and fuel droplets. It has been shown that the method can be very conveniently used to predict important parameters like fuel evaporation rate under unsteady conditions. The compatibility of the model has been confirmed against the steady state results of other workers. The numerical scheme proposed in this paper with some further work should lead to a useful computational tool to study the behaviour of air–fuel droplet flow in a practical situation, for example, in the intake manifold of a spark ignition engine.

REFERENCES

BENSON, R. S., GARG, R. D. & WOOLLATT, D. 1964 A numerical solution of unsteady flow problems. *Int. J. Mech. Sci.* **6**, 117–144.

BOAM, D. J. & FINLAY, I. C. 1979 A computer model of fuel evaporation in the intake systems of a carburetted petrol engine. *Conf. Fuel Economy and Emissions of Lean Burn Engines* C89/79, pp. 25–37.

BULIRSCH, R. & STOER, J. 1966 Numerical treatment of ordinary differential equation by extrapolation methods. *Numerische Mathematik* **8**, 1–13.

INGEBO, R. D. 1956 Drag coefficients for droplets and solid spheres in clouds accelerating in air stream. NACA TN 3762.

JENNY, E. 1950 Unidimensional transient flow with consideration of friction, heat transfer and change of section. *The Brown Boveri Review*, pp. 447–461, Nov.

LO, R. S. & LALAS, D. P. 1977 Parametric study of fuel-droplet flow in an idealized engine induction system. SAE Paper 770645.

PRIEM, R. J. & HEIDMANN, M. F. 1960 Propellant vaporization as a design criterion for rocket-engine combustion chambers. NASA TR R-67.

RANZ, W. E. & MARSHALL, W. R. 1952 Evaporation from drops. *Chem. Engng Prog.* **48**, 141–146, 173–180.

REID, R. C. & SHERWOOD, T. K. 1966 *The Properties of Gases and Liquids*, 2nd Edn, p. 124 McGraw-Hill, New York.

TRAYSER, D. A. *et al.* 1969 A study of the influence of fuel atomisation, vaporization and mixing process on pollutant emissions from motor vehicle power plants. Battelle Memorial Institute, Columbus Laboratories, PB. 185886.

YU, T. C. 1953 Fuel distribution studies—a new look at an old problem. *SAE Trans.* **71**, 596–613.

YUN, H. J., LO, R. S. & NA, T. Y. 1976 Theoretical studies of fuel droplet evaporation and transportation in a carburetor venturi. SAE Paper 760289.